J Appl Electrochem (2010) 40:79–89
DOI 10.1007/s10800-009-9983-2

ORIGINAL PAPER

Electrochemical response of the two isomers conjugated acids, maleic and fumaric, on glassy carbon electrode modified with platinum nanoparticles

F. M. El-Cheikh · F. A. Rashwan · H. A. Mahmoud · Mahmoud El-Rouby

Received: 26 February 2009 / Accepted: 16 August 2009 / Published online: 30 August 2009

Abstract Cyclic voltammetry (CV), electrochemical impedance spectroscopy (EIS), and chronoamperometry (CA) techniques are essentially used for the study of the electroreduction of the two isomers maleic and fumaric acid systems in 0.1 M KCl at 298 K. The measurements are carried out on Pt nanoparticles electrodeposited on glassy carbon electrode (GCE). The modification of the electrode enables the appearance of better resolved peaks of the cyclic voltammograms of the two isomers of the acids in comparison with the poor behavior in absence of the modification. Two well-separated reversible cathodic waves at −0.44 and −0.59 V versus Ag/AgCl are characterizing the electroreduction cyclic voltammogram of maleic acid. The electroreduction of fumaric acid shows only one reversible peak at −0.362 V versus Ag/AgCl is observed. Peak separations and current functions together with other parameters of the electrochemical behavior of both isomers are calculated and discussed. Rate parameters of the anion radicals of both isomers in 0.1 M KCl on immobilized GCE with Pt nanoparticles are obtained and discussed.

Keywords Electrodeposition · Pt nanoparticles · Electroreduction · Fumaric · Maleic

1 Introduction

Nanosized particles attracted much attention, and are currently the subjects of considerable researches. Due to their high specific surface area which makes it having unusual physical and chemical properties, nano-materials are used in the potential application and chemical separation [1]. Also, nanoparticles have been found to be used in technological applications in many different areas, such as photocatalysis [2], electrocatalysis [3], and biomedical applications [4, 5]. The electrodeposition of metal nanoparticles onto carbon electrodes has become the interest of a large number of researches [6–10]. Platinum nanoparticles dispersed onto smooth, non-active surfaces are of interest for the catalytic activity of Pt toward reactions of interest in fuel cell. Electrodeposition of platinum deposits produced during the electroreduction of $PtCl_6^{2-}$ complex in acid solutions has a much enhanced surface [11]. Catalytic activity is one of the most important properties of Pt nanoparticles; therefore, it is used to enhance the reaction efficiency. Pt-based materials are still recognized as the most effective catalysts [12]. Due to the biological and industrial importance of maleic and its isomer acid (fumaric), the electrochemical behavior of them was studied in this article. Furthermore, little studies covering the area of the two isomers maleic and fumaric acids have been carried out [13–16]. Moreover, almost totally rare studies using GCE immobilized with Pt nanoparticles were undertaken. Recently, controlled potential electrolysis was employed to accomplish homopolymerization of maleic anhydride by direct electron transfer [17]. The transformation of di-ethylmaleate to di-ethylfumarate has been studied electrochemically [18]. Another study proved that the electroreduction of maleic and fumaric acids proceeds via the cleavage of the carbon–carbon π bond converting to succinic [14]. In this study, we present an application of the relatively new trend of modifying electrodes. Accordingly, in this report, detailed investigations of the electroreduction behavior of maleic acid and its isomer in 0.1 M KCl

F. M. El-Cheikh · F. A. Rashwan · H. A. Mahmoud · M. El-Rouby (✉)
Chemistry Department, Faculty of Science, Sohag University, Sohag 82524, Egypt
e-mail: dr_mahmoudelrouby@hotmail.com

on Pt-nanoparticle electrodeposits are carried out. Cyclic voltammetric, electrochemical impedance, and related techniques were combined to obtain the desired data.

2 Experimental

2.1 Chemicals

Both maleic and fumaric acids were purchased from (BDH). Solutions of 0.1 M potassium chloride, 0.5 M Na_2SO_4 (BDH), 0.1 M potassium nitrate, and a stock 0.1 M of potassium hexacyanoferrate (III) were freshly prepared by dissolving the appropriate amounts in bidistilled water. A 0.5×10^{-3} and 1×10^{-3} M solution of di-hydrogen tetrachloroplatinate (Aldrich) were freshly prepared by dissolving the appropriate amount in a 0.1 M potassium chloride.

2.2 Apparatus and equipments

All electrochemical experiments were performed with an EG&G PARC Potentiostat/Galvanostat model 273 A. The EIS measurements were performed with a lock-in analyzer (Model 5208) coupled with a potentiostat/galvanostat (model 273) from EG&G Instruments. The model 378 software was used for EIS measurements. A conventional three-electrode cell system was used, consisting of a bare or modified glassy carbon (3 mm in diameter) as a working electrode, platinum sheet as an auxiliary electrode, and the Ag/AgCl is the reference electrode. All experiments were thermostated at 298 ± 0.2 K. Surface analysis of the modified electrodes were carried out using a JEOL JSM-5500 LV Scanning Electron Microscope (JOEL, Japan), at an acceleration voltage of 5 keV and a working distance of 4–5 mm. Image analysis were performed visually and with common software (ImageJ, Wright Cell Imaging Facility, Toronto Western Research Institute, University Health Network) for particle counting and particle size.

2.3 Preparation of the modified electrode

Prior to the electrodeposition of Pt nanoparticles, the glassy carbon electrode surface was polished first with no. 2000 emery paper, then with aqueous slurries of successively finer alumina powder with the help of polishing microcloth. Then, it was rinsed with doubly distilled water. The bare GCE was, then, sonicated for 10 min in bidistilled water bath. Electrodeposition process was accomplished by scanning between 0.15 and −0.9 V versus Ag/AgCl, at a scan rate of 0.05 V s^{-1} for 25 cycles in a fresh solution of 0.1 M KCl containing either 0.5 or 1 mM of H_2PtCl_6, according to the required condition of the experiment. The delay time of the deposition step was varied from 0 to 60 s to obtain Pt deposits with different characteristics.

3 Results and discussion

3.1 Pt nanoparticles electrodeposition

Figure 1 provides a general shape of a reversible cyclic voltammogram for the reduction of Pt(IV) in 0.1 M KCl on the GCE obtained by continuous scanning between 0.15 and −0.9 V versus Ag/AgCl.

One clearly resolved reversible peak at −0.42 V versus Ag/AgCl is observed. This wave is attributed to the reduction of Pt(IV) to the Pt metal on the surface of the GCE [5, 19].

It is found that the increase of either the delay time of deposition or the concentration of the $PtCl_6^{2-}$ leads to an increase in the average particle size of the Pt nanoparticles [6, 20].

3.2 Pt nanoparticles characterization

3.2.1 Scanning electron microscopy analysis characterization

Scanning electron microscopy (SEM) images of the Pt nanoparticles electrodeposited onto the GCE under different operating conditions are shown in Fig. 2a–d. The SEM images show that the deposited Pt particles are in the nanoscale size and homogeneously distributed throughout

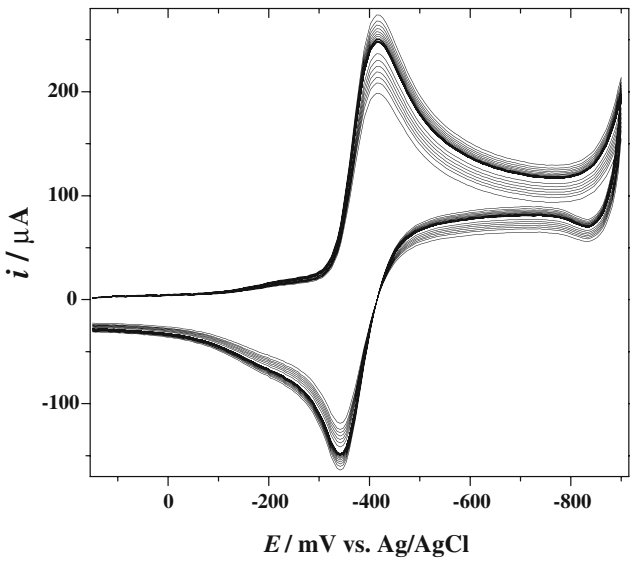

Fig. 1 Preparation of platinum nanoparticle-modified glassy carbon electrode by continuous scanning cyclic voltammetry on GCE immersed in solution contains 0.1 M KCl and 0.5×10^{-3} M H_2PtCl_6 solution at 298 K ($v = 0.05$ V s^{-1}) for 25 cycles

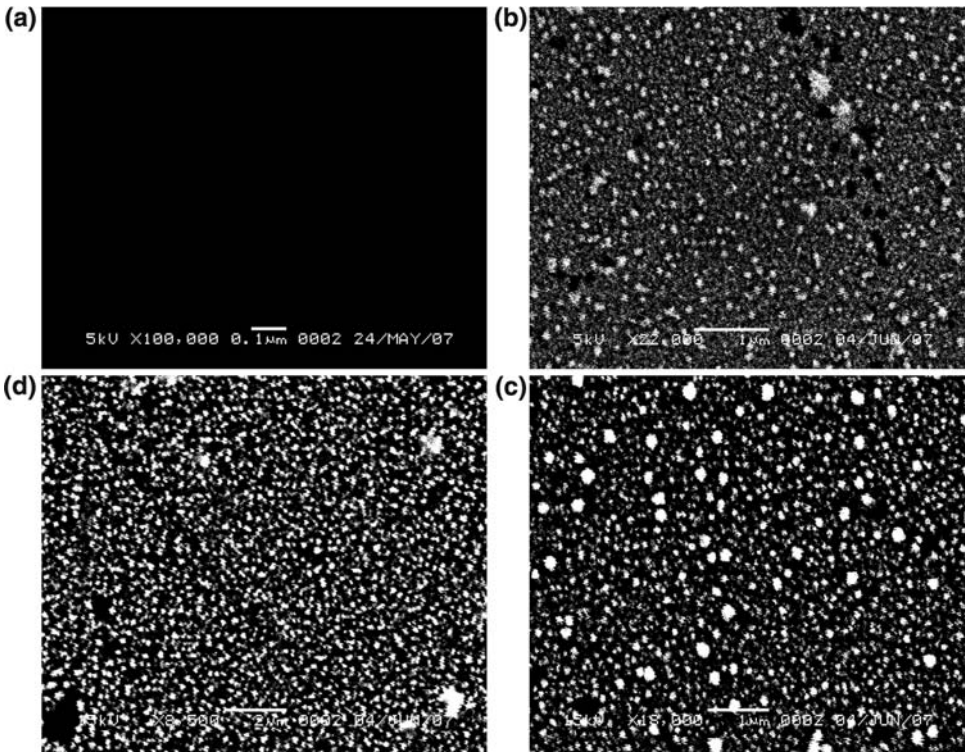

Fig. 2 SEM images of bare GCE (**a**) and electrochemically deposited Pt nanocrystallites on GCE; delay time 0 s and 0.5×10^{-3} M H_2PtCl_6 solution, (**b**); delay time 60 s and 0.5×10^{-3} M H_2PtCl_6 solution, (**c**) Delay time 0 s and 1×10^{-3} M H_2PtCl_6 solution (**d**) at 298 k

the GC surface. The Pt nanocrystals in the SEM images appear as circular bright spots surrounded by a textured background of darker GC substrate. It is clear from these images that the increase of either the delay time of deposition or the concentration of the $PtCl_6^{2-}$ resulted in an increase in the average particle size of the Pt nanoparticles [20], and as confirmed by the precise calculations of the ImageJ program. It has been shown that the low concentration bath (0.5 mM K_2PtCl_6), yields a low number density with a lot of nanocrystals (~70%) with small size (~10 nm). The other particles having 20 nm average size (Fig. 2b).

At the higher concentration (1.0 mM H_2PtCl_6), a high number density of relatively monodisperse particles are deposited with increasing the size. Small size particles (~32 nm) of ~49% coexisting with small number (~10%) of large size particles (~68 nm) and 20% of a size (~120 nm) as shown in Fig. 2d. This reflects both an increase of the active sites on the surface of GCE (increasing the Pt loading) and nucleation growth.

The increase of the deposition time from 0.0 to 60 s leads to both an increasing in the particle size and an increasing in the particle number density. A 30% of large size particles have 60–88 nm range, and a 17% of the particles have 150–300 nm size range, these large particles are observed coexisting with lots of (~53%) smaller size nanoparticles (~15 nm) as shown in Fig. 2c. This means that the nucleation growth is favored over the establishment of new deposition active sites. SEM image analyses for nanoparticles are summarized in Table 1.

Furthermore, both the real surface area of the Pt loading on GCE/cm^{-2} and the mass specific surface area (cm^2 μg^{-1}), were calculated by two methods, such as SEM analysis and mass transfer method [21]. The data of both methods are found to be in agreement with each other. A behavior which is similar to that observed in the literature [22–24].

3.2.2 *Cyclic voltammetric characterization*

Cyclic voltammetry (CV) of electroactive species $Fe(CN)_6^{3-/4-}$ is a standard example for testing the kinetic barrier of the interface and is to estimate the real active surface area of the electrodes [25, 26].

Figure 3 shows CV response of bare and modified GCE with Pt nanoparticles in 0.1 M KCl aqueous solution contain 5 mM $[Fe(CN)6]^{4-/3-}$ at a scan rate of 0.05 Vs^{-1}.

Noticeable that well-defined cyclic voltammograms are observed at the modified GCE with a peak-to-peak separation (ΔE_p) of about ~0.070 V (Fig. 3b–d). An obvious increase in anodic and cathodic peak currents is observed by decreasing the Pt loading or by decreasing the particle size deposits. A quasi-reversible CV was obtained with a peak-to-peak separation (ΔE_p) of 0.318 V when bare GCE is used (Fig. 3a). A decreasing in anodic and cathodic peak currents compared with the CV on the modified electrodes are observed.

Table 1 Physical characteristics parameters determined from voltammetric measurements and SEM analysis for Pt nanoparticles electrodes

Electrode no.	Q[a] (μC)	Pt loading[b] (g cm^{-2}) × 10^5	Real surface area of Pt loading[c] (cm^2)		Specific surface area[d] (cm^{2}μg^{-1})		Roughness factor[e]	Mean Diameter[f] (nm)
			SEM method	Mass transfer method	SEM method	Mass transfer method		
b	636.68	1.79	1.20	0.300	94.82	95.61	3.13	15 ± 2
c	772.91	2.21	1.46	0.240	93.25	80.00	2.50	38 ± 2
d	878.43	2.51	1.60	0.180	90.20	71.57	1.88	180 ± 2

[a] Net cathodic charge passed in Pt deposition

[b] Calculating Pt loading assuming 100% current efficiency

[c] As estimated from SEM analysis and mass transfer methods

[d] Mass specific surface area: Surface area per unit weight of Pt

[e] Surface area of Pt per unit area of GCE

[f, g] Data measurements based on ImageJ program software

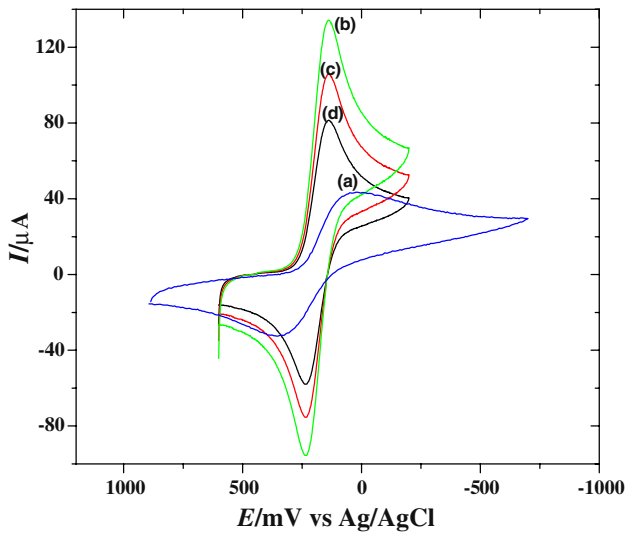

Fig. 3 CV of 5 × 10^{-3} M [Fe (CN)$_6$]$^{-3/-4}$ in 0.1 M KCl on bare GCE (*a*) and the modified GCE with Pt nanoparticles at different loads of Pt nanoparticles; 1.79 × 10^{-5} (*b*), 2.21 × 10^{-5} (*c*), and 2.51 × 10^{-5} g cm^{-2} (*d*) at v = 50 mV s^{-1} at 298 k

Moreover, the peak currents of CV obtained on the modified electrodes (Fig. 3b–d) are proportional to the square root of scan rate. This implies that the redox process is controlled via diffusion phenomena.

The real active surface area can be estimated by using Randles equation [26, 27]:

$$i_p = 3.01 \times 10^5 n^{3/2} \alpha^{1/2} D^{1/2} A_{rsa} c_o |v|^{1/2} \quad (1)$$

where n is the number of electrons transferred in the redox reaction, v is the scan rate of the potential (V s^{-1}), A_{rsa} is the real surface area of the electrode (cm^2), D is the diffusion coefficient of the species in the solution (cm^2 s^{-1}), which is subsequently determined from chronoamperometric measurements, c_o is the bulk concentration of the probe molecule in solution (mol cm^{-3}), i_p is the peak current of the redox couple (A), and α the electron transfer coefficient. The value of the electron transfer coefficient is assumed to be 0.5 for ferri/ferrocyanide redox couple.

Heterogeneous charge transfer rate constant (k_s) for this reaction can be obtained, according to the following equation [28]:

$$\psi = \frac{(D_0/D_R)^{\alpha/2} k_s}{\pi D_0 v (nF/RT)^{1/2}} \quad (2)$$

Using the ΔE_p value and the working curve of Nicholson [29] to obtain the transfer parameter (ψ) and then the heterogeneous charge transfer rate constant (k_s) for the electron transfer process. The mean values of k_s is found to be 1.50 × 10^{-2} and 1.08 × 10^{-3} cm s^{-1} on both the modified and the bare GC electrode, respectively. Indicating the facile nature of the charge transfer at the Pt nanoparticles electrodes.

3.2.3 *Chronoamperometric characterization*

Chronoamperometry (CA) is used, in this case, for the determination of the diffusion coefficient of the species and investigating the kinetics of the charge transport on the modified electrodes. Figure 4 shows the chronoamperograms for the GCE/Pt$_{nano}$ electrodes with different Pt loadings in the presence and absence of ferricyanide. The first and second working electrode potentials were adjusted at 0.600 and 0.128 V (vs. Ag/AgCl), respectively.

The diffusion coefficient can be obtained using the relation between current decay and time, as in Cottrell equation [18, 28]:

$$i = nFAD^{1/2} c_o \pi^{-1/2} t^{-1/2} \quad (3)$$

where n is the number of electrons transferred, F the Faraday constant (96,484 C mol^{-1}), A is the electrode surface

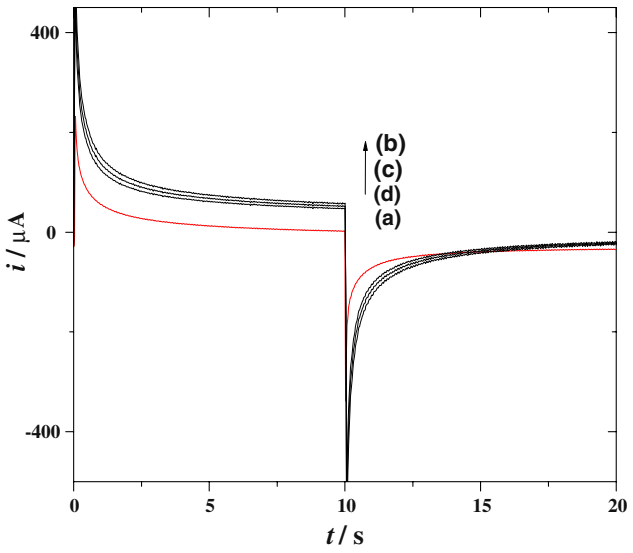

Fig. 4 The double step potential chronoamperograms obtained at bare GCE (*a*) and modified with Pt nanoparticles for 5×10^{-3} M $K_3[Fe(CN)_6]$ in 0.1 M KCl at $\tau = 10$ s with different loads of Pt nanoparticles; 1.79×10^{-5} (*b*), 2.21×10^{-5} (*c*), and 2.51×10^{-5} g cm^{-2} (*d*) at 298 k

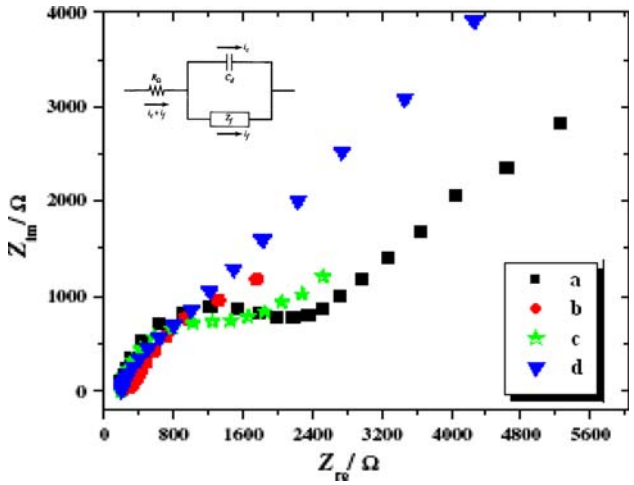

Fig. 5 Complex impendence plane plot of bare GCE (*a*), and modified GC with Pt_{nano} electrodes with different loads of Pt nanoparticles; 2.21×10^{-5} (*b*) 2.51×10^{-5} g cm^{-2} (*c*) and 1.79×10^{-5} (*d*) for 5.0×10^{-3} M $Fe(CN)6^{3-/4-}$ in 1.0 M KCl. At the cathodic peak potential. AC amplitude at 0.005 V, the frequencies from 100 KHz to 5 Hz at 298 k. Inset (*top*) is the Randle's equivalent circuit

area (cm^2), c_o is the bulk concentration (mol/cm^3), i is the current (A), t is the time elapsed (s), and D the diffusion coefficient (cm^2 s^{-1}).

The plots of i versus $t^{-1/2}$ give straight lines, and the D mean value is found $\sim 7.2 \times 10^{-6}$ cm^2 s^{-1} for the ferricyanide ion [30]. The plots of $it^{1/2}$ versus t for a known concentration of ferricyanide show that $it^{1/2}$ function is constant and time independent over a wide range of the experiment time. This confirms the foregoing suggestion that the electron transfer process is under diffusion control. In addition, the catalytic rate constant (k_{cat}) for ferricyanide on the GCE/Pt_{nano} was calculated using Galus method, by the equation [24]:

$$\frac{i_{cat}}{i_l} = \pi^{1/2}(k_{cat}c_o t)^{1/2} \quad (4)$$

where i_{cat} is the catalytic current of ferricyanide on the modified electrode, i_l the limiting current in absence of ferricyanide, c_o the bulk concentration (mol/cm^3) and t the time elapsed. The slope of i_{cat}/i_l versus $t^{1/2}$ gives k_{cat} of mean value of about 3.98×10^3 M^{-1} s^{-1}. This value of k_{cat} explains the catalytic nature of the surface of the modified electrode.

3.2.4 Electrochemical impedance spectroscopy (EIS) characterization

Electrochemical impedance spectroscopy (EIS) is an effective and very sensitive method for probing the features of surface of modified electrodes [31–33]. In order to investigate the electrical properties of the electrodes/solution interfaces, the Randle's equivalent circuit can be chosen to represent the electroreduction process in this case (Fig. 5).

As shown in Fig. 5, the EIS spectra is presented as Nyquist plot for the bare and the modified GCE of different loading of Pt Nanoparticles for 5 mM ferricyanide in 0.1 M KCl at the cathodic peak potential at 298 K. The charge transfer resistance (R_{ct}) exhibits the electron transfer kinetics of the redox-probe at the electrode/electrolyte interface. It can be represented as a semicircle in the complex plane plot of Z_{im} against Z_{re}. R_{ct} has the greatest value $\sim 2{,}000$ Ω at the bare GCE in the test solution, the R_{ct} decreased dramatically when Pt nanoparticles were deposited on the GCE electrode. By increasing the Pt loading or particle size, the R_{ct} increases. R_{ct} is decreased to 200 Ω at the modified GCE with the smallest Pt nanoparticles (Fig. 5b). This implies that the Pt nanoparticles play an important role in the conductivity improvement, which facilitates the electron transfer, and the electrode gets working with high efficiency after modification.

3.3 Electrochemical response of maleic acid on the Pt nanoparticles modified electrode

3.3.1 Cyclic voltammetry

Figure 6 presents cyclic voltammograms of 1.25 mM Maleic acid obtained in 0.1 M KCl on both bare and modified GCE with Pt nanoparticles. Two good resolved reversible cathodic waves on the modified GCE at −0.44 and −0.59 V versus Ag/AgCl are observed. On the bare

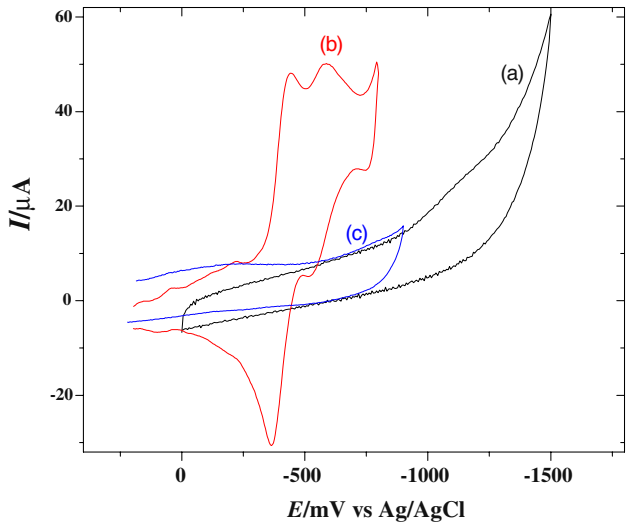

Fig. 6 CV (in presence) of 1.25 mM maleic acid in 0.1 M KCl at $v = 0.1$ V s^{-1} at 298 K on bare (*a*), modified GCE with Pt nanoparticles at load of 2.21 × 10^{-5} g cm^{-2} (*b*) and modified GCE with Pt nanoparticles in 0.1 M KCl in absence of maleic acid (*c*)

GCE, no significant peaks under the same conditions are detected.

The cathodic peak potentials E_{pc}, peak currents, peak separations (ΔE_p), and the criteria of current functions $i_p/v^{1/2}$ at different scan rates for the electroreduction of maleic acid at the first peak on GCE modified with Pt nanoparticles are summarized in Table 2.

Peak separations clearly suggest that the reaction is reversible one electron transfer process at the first peak, according to the relation [28]:

$$\left|E_{pc} - E_{pa}\right| = \frac{2.2RT}{nF} = \frac{56.5}{n}\text{mV} \quad (5)$$

A linear relation between the peak current (i_p) and the square root of the scan rate reveals that the electron transfer process is controlled via a diffusion step.

Despite current function ($i_p/v^{1/2}$) decreases with increasing the scan rate, one may conclude the presence of a chemical reaction coupled to the electron transfer process (EC mechanism; Table 2).

Heterogeneous charge transfer rate constant (k_s) for the charge transfer step can be obtained, according to Eq. 2 and using the method mentioned above. The value of k_s for the electroreduction of maleic under these conditions, amounts ~0.14 cm s^{-1}, by assuming $\alpha \approx 0.5$.

3.3.2 Double potential step chronoamperometry

Chronoamperometry (CA) is an important method for the characterization of the EC mechanism and also for the determination of the rate constant of follow-up chemical reactions [34]. Therefore, this method was applied in this study and again employed for the determination of the diffusion coefficient. It is known in chronoamperometric measurements that the i_a/i_c ratio should be equal to unity in absence, but less than unity in the presence of follow-up chemical reaction.

Figure 7a, b shows the double potential step chronoamperograms at both the first and the second cathodic peak potentials of maleic acid. In the case of maleic, this figure reveals that the i_a/i_b ratio is less than unity. This is due to the presence of electron transfer process followed by a chemical reaction (EC mechanism).

Moreover, the diffusion coefficient can be obtained by the relation between current decay and time as in Cottrell equation (3). The diffusion coefficient of maleic acid obtained by this method is of the order 8.50 × 10^{-7} cm^2 s^{-1}.

Also, the rate constant of the homogeneous chemical reaction (k_c) following the first charge transfer can be obtained by working curves (relation between i_a/i_b as a function of $k\tau$ and $((t - \tau)/\tau)$ [35]. The rate of coupled chemical reaction of maleic acid at the first cathodic peak after the electron transfer process is found to be ~0.080 s^{-1}. The plots of $it^{1/2}$ versus t for first and second peaks of maleic show that $it^{1/2}$ is constant and time independent. This assumes again the diffusion-controlled electron transfer process.

3.3.3 Electrochemical impedance spectroscopy

Figure 8 shows the Nyquist plots of the impedance spectroscopy on the modified Pt nanoparticles electrodes, measured from 6.31 Hz to 100 kHz at the first and second cathodic potential peaks of the voltammogram for maleic acid. In the case of the presence of a chemical reaction following the charge transfer process, the Randles equivalent

Table 2 Cyclic voltammetric data for the electroreduction of 1.25 mM maleic acid on the GCE/Pt nanoparticles electrode at load of 2.21 × 10^{-5} g cm^{-2} in 0.1 M KCl at 298 K (first wave)

Scan rate (mV s^{-1})	$-E_{pc}$ (V)	i_{pc} (μA)	$i_p/v^{1/2}$ (μA mV^{-1} s$^{1/2}$)	ΔE_P (mV)
50	0.437	39.94	5.65	88.70
100	0.440	47.73	4.77	111.00
200	0.447	59.41	4.20	131.08
300	0.452	67.07	3.87	139.70
400	0.459	73.44	3.67	145.00
500	0.464	79.32	3.55	152.24

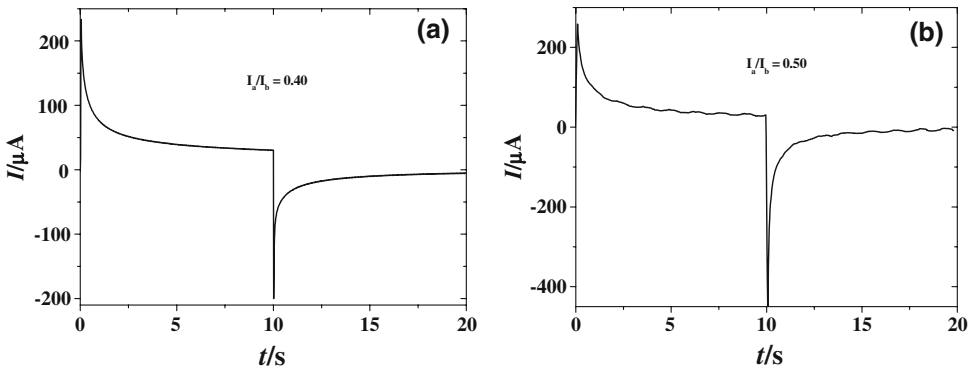

Fig. 7 Double potential step chronoamperograms obtained at GCE modified with Pt nanoparticles at load of 2.21×10^{-5} g cm^{-2}, for 1.25×10^{-3} M maleic acid in 0.1 M KCL, **a** at first peak $E_i = 0.0$ V, $E_s = -0.44$ V, and $E_f = 0.0$ V and **b** at second peak $E_i = 0.0$ V, $E_s = -0.60$ V, and $E_f = 0.0$ V, at $\tau = 10$ s, at 298 k

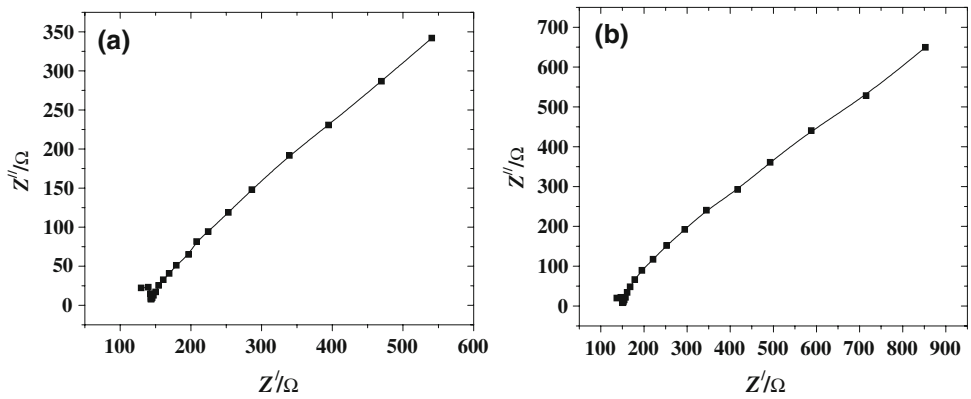

Fig. 8 Complex impedance plane plot at modified with Pt nanoparticles at load of 2.21×10^{-5} g cm^{-2} for solution containing 1.25×10^{-3} M maleic acid at first cathodic peak (**a**) and second cathodic peak (**b**) in 0.1 M KCL, AC amplitude at 0.005 V, The frequencies from 100 KHz to 5 Hz, at 298 K, versus Ag/AgCl

circuit is not sufficient to describe the case, thus it should be assumed the presence of an additional impedance contribution connected with the coupled chemical reaction following the electron transfer process.

The Ohmic resistance of the solution (R_s), the charge transfer resistance (R_{ct}) at the electrode/electrolyte interface, and the double layer capacitance (C_{dl}), were calculated from the Bode plot and are listed in Table 3. Noticeable that the R_{ct} in the case of maleic for both the first and the second electron transfers are considerably small, but the C_{dl} is relatively high. This can be interpreted on the basis that the electron transfer processes during the electroreduction of maleic acid are easy to occur.

It is known that an EIS measurement is frequently used for the determination of the kinetic parameters of electrochemical processes [27, 36, 37]. The EIS data is used for the determination of the heterogeneous rate of electron transfer, by using the simplified equation:

$$\cot\phi = 1 + \frac{\sqrt{D}}{2k_s}\sqrt{\omega} \tag{6}$$

where ϕ is the phase angle, D is the diffusion coefficient of species, assumed to be equal for both redox forms, k_s is the heterogeneous rate constant of the electron transfer, and ω angular frequency, by assuming $\alpha = \beta = 0.5$.

The dependence of the square root of the angular frequency on cotϕ, as shown in Fig. 9 illustrate some deviation at low frequencies, indicating the presence of an EC process [37].

The heterogeneous rate constants of electron transfer reaction for maleic are obtained by this method and registered as of $\sim$0.15 and $\sim$0.06 cm s^{-1}, respectively. These values are consistent with those obtained from CV measurements, and the values fall within the range of Nernestian behavior.

Table 3 EIS data was obtained for the electroreduction of 1.25 mM Maleic at first and second cathodic peaks

Substance	R_s (Ω)	R_{ct} (Ω)	C_{dl} f $\times 10^5$	Φ angle
Maleic at first peak	128.80	91.20	136.00	46.30
Maleic at second peak	128.40	372.41	87.20	45.50

3.4 Electrochemical response of fumaric acid on the Pt nanoparticle-modified electrode

3.4.1 Cyclic voltammetry

Figure 10 shows the electroreduction of fumaric acid under the same conditions as those of maleic acid. It is clear that, in the reverse scan, the position of the oxidation peak of fumaric acid lie very near to the position of the oxidation of

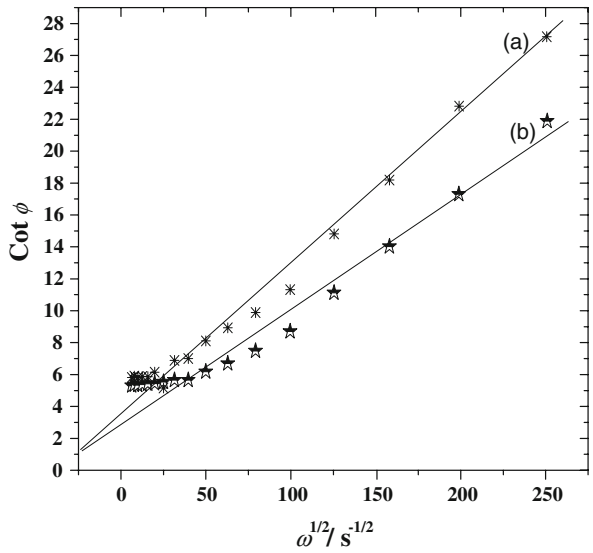

Fig. 9 Dependence of the faradic phase angle on the square root of angular frequency derived from EIS data is measured for 1.25×10^{-3} M maleic at (*a*) first cathodic peak (*b*) second cathodic peak in 0.1 M KCL at Pt nanoparticles electrode at load of 2.21×10^{-5} g cm^{-2} at 298 K versus Ag/AgCl

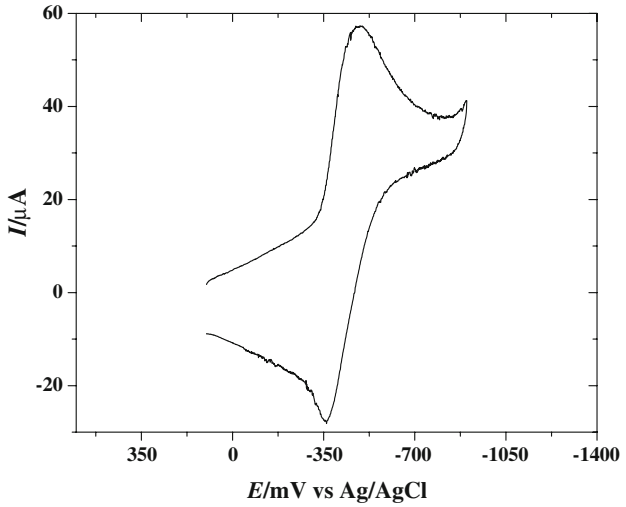

Fig. 10 CV of 1.25×10^{-3} M Fumaric acid in 0.1 M KCL on the bare GCE modified with Pt nanoparticles at load of 2.21×10^{-5} g cm^{-2}, at $v = 0.1$ V s^{-1}, at 298 K

the first peak of maleic acid, both at approximately −0.362 V. This is clear evidence that the reduced maleic acid radical anion transforms into the more stable fumaric acid radical anion through a conformation process.

The peak separations, reduction peak potentials, peak currents, and the criteria of the current function at different scan rates for the electroreduction of fumaric are summarized on the modified electrode in Table 4. The peak current of the electroreduction of fumaric acid varies linearly with the root of the scan rates. This indicates that the process is governed by diffusion-controlled phenomena. The peak separations are somewhat large indicating the quasi-reversibility of electron transfer process. This means that the radical anion of fumaric is stable within the time scale of the CV experiment. The criteria of the current function $i_p/v^{1/2}$ are almost constant with increasing the scan rate of pure charge transfer.

Heterogeneous charge transfer rate constant (k_s) for this reaction can be obtained, according to Eq. 2. Using the method above, k_s for the electroreduction of fumaric under these conditions, is evaluated which accounts to ~ 0.06 cm s^{-1}, also by assuming $\alpha \approx 0.5$. This value indicates that the rate of electron transfer for the electroreduction process of fumaric acid is considerably fast and clearly under diffusion-controlled phenomena, but less than those of maleic acid. The small differences in the heterogeneous rate constants of electron transfer between maleic and fumaric would be due to the difference in their geometric structures and the diffusion coefficients.

3.4.2 *Double potential step chronoamperometry*

Figure 11 shows the double potential step chronoamperograms obtained at GCE modified with Pt nanoparticles for 1.25 mM fumaric acid in 0.1 M KCl, $E_i = 0.0$ V, $E_s = -0.63$ V, and $E_f = 0.0$ V at $\tau = 10$ s at 298 K.

The i_a/i_c ratio nearly equals to the unity assuming the possibility of the absence of chemical reaction following the electron transfer process. The diffusion coefficient of fumaric obtained by the above method has a value of 2.88×10^{-7} cm^2 s^{-1}. This value is somewhat smaller than that of maleic acid, verifying that fumaric acid may be affected by its steric-hindrance that influencing affects its diffusion toward the electrode.

Moreover, $it^{1/2}$ versus t plot for fumaric shows that $it^{1/2}$ is constant and time independent. This indicates that the electron transfer process is solely controlled by a diffusion process.

3.4.3 *Electrochemical impedance spectroscopy*

Figure 12 shows the Nyquist plot of the impedance spectroscopy of fumaric acid on the modified Pt nanoparticles electrodes, measured from 6.31 Hz to 100 kHz at the cathodic peak potential. The Randles equivalent circuit is sufficient for the description of this case.

The data reveals that at low frequencies, a linear impedance locus with an angle of $\sim 45°$ to the real axis, with a very small partially resolved semi-circle at high frequencies. This may be attributed to the presence of a relaxation occurring at the solution/electrode interface which indicates a diffusion-controlled charge transfer process. The Ohmic resistance of solution (R_s) and the

Table 4 Cyclic voltammetric data for the electroreduction of 1.25 mM fumaric acid on the GCE/Pt nanoparticles electrode at load of 2.21×10^{-5} g cm^{-2} in 0.1 M KCl at 298 K

Scan rate (mV s^{-1})	$-E_p^c$ (V)	i_p^c (μA)	$E_{p/2} - E_p$ (mV)	$i_p/v^{1/2}$ (μA mV^{-1} s$^{1/2}$)	ΔE_P (mV)
50	0.6240	26.60	80.20	3.67	150.00
100	0.6299	36.66	79.80	3.66	155.00
200	0.6529	46.00	85.43	3.25	200.00
300	0.6603	60.60	90.62	3.48	225.00
400	0.6790	68.74	95.66	3.39	255.53
500	0.6997	78.30	98.22	3.46	271.00

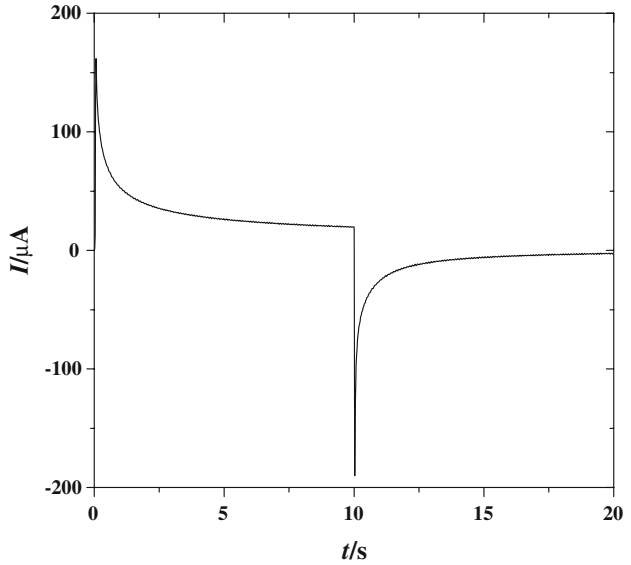

Fig. 11 Double potential step chronoamperograms obtained at GCE modified with Pt nanoparticles at load of 2.21×10^{-5} g cm^{-2} for 1.25×10^{-3} M fumaric acid in 0.1 M KCL, $E_i = 0.0$ V, $E_s = -0.63$ V, and $E_f = 0.0$ V, at $\tau = 10$ s, at 298 K

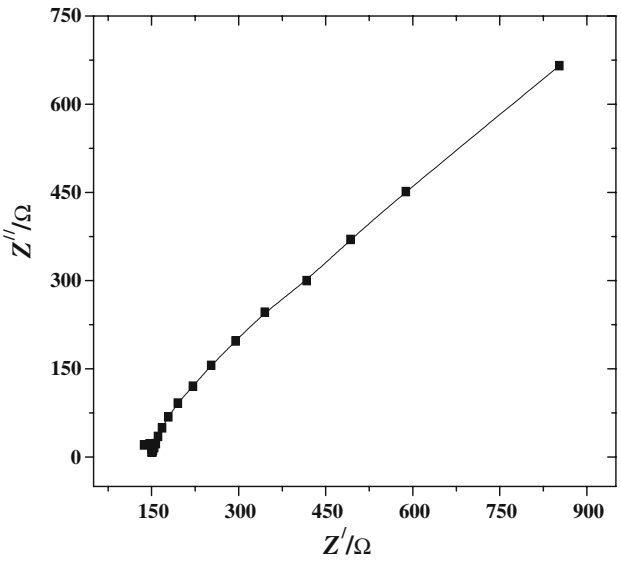

Fig. 12 Complex impedance plane plot at modified with Pt nanoparticles at load of 2.21×10^{-5} g cm^{-2} of a solution containing 1.25×10^{-3} M fumaric acid at the cathodic peak versus Ag/AgCl in 0.1 M KCL, AC amplitude at 0.005 V. The frequencies from 100 KHz to 5 Hz, at 298 K

charge transfer resistance (R_{ct}) at the electrode surface and the double layer capacitance (C_{dl}) are determined and listed in Table 5. The R_{ct} in the case of maleic acid is found less than that of fumaric acid. This demonstrates that the electron transfer process at the electroreduction of maleic is easier than that of fumaric. Again, the straight line obtained at high frequencies, in the case of fumaric acid, has unity slope, i.e., characteristic of a pure electron transfer process, E-mechanism. This verifies that the process is also a diffusionally controlled one.

Figure 13 shows the dependence of the reciprocal of the square root of the angular frequency on cotϕ of 1.25 mM fumaric acid in 0.1 M KCl on the GCE modified with Pt nanoparticles. Noticeable that small deviation from linearity at low frequencies which is indicative of the presence of pure electron transfer process, which is the prevailing one [37].

Table 5 EIS data was obtained for the electroreduction of 1.25 mM fumaric acid at 298 K same condition as Fig. 13

substance	R_s, Ω	R_{ct}, Ω	$C_{dl.}$ f $\times 10^{-5}$	Φ angle
fumaric	140.40	300.41	93.20	44.50

The heterogeneous rate constant of electron transfer for fumaric obtained by this method, has a value of 0.055 cm s^{-1}, and which is nearly in agreement with that obtained from CV data.

In this study, the possible rout for the electroreduction mechanism of maleic acid can be concluded, where the electroreduction of maleic acid is first reduced with one electron forming the radical anion. This radical passes though two competitive processes occurring at the same time. The predominant process is the isomerization reaction, i.e., maleic radical transforms to fumaric radical, which is concluded to be the more stable. Whereas the second minor process is the dimerization of the radical monomer with a neutral maleic monomer. This occurs at the first wave (EC mechanism), but at the second wave, the resultant dimmer radical anion is reduced with one another electron to form the di-anion of the dimmer that may be

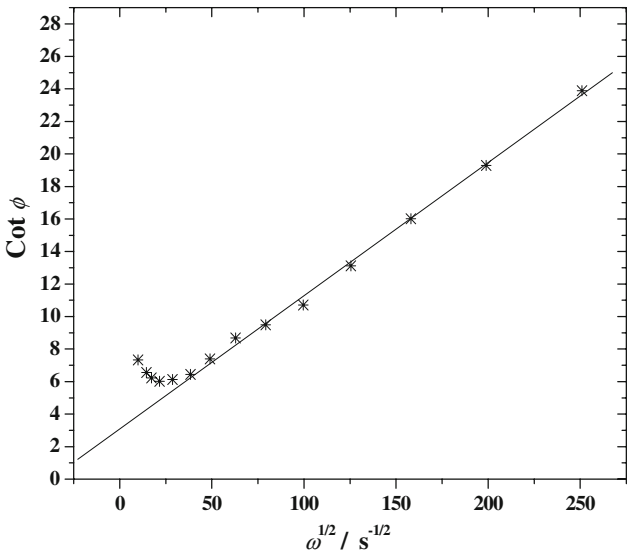

Fig. 13 Dependence of the faradic phase angle on the square root of angular frequency derived from EIS data measured for 1.25×10^{-3} M fumaric at the cathodic peak in 0.1 M KCL at Pt nanoparticles electrode at load of 2.21×10^{-5} g cm^{-2} at 298 K versus Ag/AgCl

partially protonated. This was confirmed with CV, CA, and an EIS technique, i.e., the expected rout for the electroreduction mechanism is that as follows:

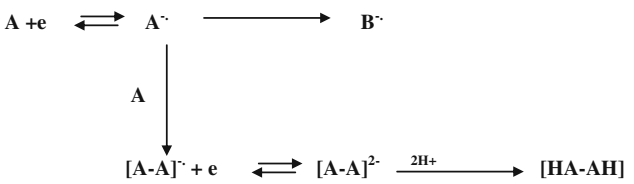

where **A** and $\mathbf{A}^{-\cdot}$ are maleic and its radical anion, respectively, $\mathbf{B}^{-\cdot}$ fumaric radical anion, $[\mathbf{A}–\mathbf{A}]^{-\cdot}$ dimmer radical, and **AH–AH** is the protonated dimer.

4 Conclusions

(1) The modified GC electrodes with Pt nanoparticles were prepared in our laboratory by easy and fast method, as sensor for the electroreduction of both maleic and fumaric acids.
(2) The prepared electrodes were investigated and examined by different tools. SEM analysis showed the electrodeposited Pt particles in the range of nanometer size.
(3) The size and the number density of the electrodeposits increase by increasing the electrodeposition, delay time, and the concentration.
(4) CV, CA and EIS measurements reveal the high catalytic activity of the prepared electrodes.
(5) The electroreduction of both maleic and fumaric acids on the modified electrode with Pt nanoparticles is much more improved than that on the bare GCE.
(6) CV, CA, and EIS measurements confirm that the electroreduction of maleic acid proceeds via EC and E-mechanisms for fumaric acid.
(7) The electroreduction mechanism of maleic acid includes two competitive chemical processes occurring at the same time after the electron transfer process. The predominant one is that the maleic radical anion can be isomerized transforming to the *cis* isomer. Whereas the other minor process is that the maleic radical combine with a neutral one forming a dimmer that can be reduced.

Acknowledgments The authors gratefully acknowledge the Chemistry Department, Faculty of Science, Sohag University for financial support. The authors also thank the Technician of Qena University for assistance in obtaining the SEM images.

References

1. Jiang J, Kucernak A (2002) J Electroanal Chem 520:64
2. Zhao DA, Peng TA, Liu MA, Lu LA, Cai P (2008) Microporous Mesoporous Mater 114:166
3. Feng JJ, Zhao G, Xu JJ, Chen HY (2005) Anal Biochem 342:280
4. Mürbe J, Rechtenbach A, Töpfer J (2008) Mater Chem Phys 110:110
5. Wang S, Yin Y, Lin X (2004) Electrochem Commun 6:259
6. Finot MO, Braybrook GD, Mcdermott MT (1999) J Electroanal Chem 466:234
7. Zoval JV, Biernacki PR, Penner RM (1996) Anal Chem 68:1585
8. Zoval JV, Stiger RM, Biernacki PR, Panner RM (1996) J Phys Chem 100:837
9. Zoval JV, Lee J, Gorer S, Panner RM (1998) J Phys Chem B 102:1166
10. Chen Z, Li J, Wang E (1994) J Electroanal Chem 373:83
11. Kravtsov VI (2000) Russ J Electrochem 36:1209
12. Xu Y, Lin X (2007) Electrochim Acta 52:5140
13. Kvaratskheliya R, Kvaratskheliya E (2000) Russ J Electrochem 36:909
14. Gulaboski R, Spirevska I, Soptrajanova L, Slavevska R (2001) Anal Lett 34:1719
15. Warshowsky BJ, Elving PJ, Mandel J (1941) Anal Chem 19:161
16. Elving PJ, Rosenthalz I (1954) Anal Chem 26:1454
17. Akbulut U, Hacioglu B (1991) J Polym Sci A 29:219
18. Greef R, Peat R, Peter LM, Pletcher D, Robinson J (1985) Instrumental method in electrochemistry. Ellis Horwood Limited, Chichester
19. Xian Y, Zhang W, Xue J, Ying X, Jin L, Jin J (2000) Analyst (Lond) 125:435
20. El-Deab MS, Okajima T, Ohsaka AT (2003) J Electrochem Soc 150:A851
21. Trasatti S, Petrii OA (1991) Pure Appl Chem 63:711
22. Ye J, Fedkiw PS (1996) Electrochim Acta 41:221
23. El-Deab MS, Sotomura T, Ohsaka T (2005) Electrochem Commun 7:29
24. Gopalan AL, Lee KP, Manesh KM, Santhosh P, Kim JH (2006) Catal Chem 256:335
25. Forker W (1989) Electrochemistry. Akademie-Verlag, Berlin

26. Lu Y, Yang M, Qu F, Shen G, Yu R (2007) Bioelectrochemistry 71:211
27. Hrapovic S, Lui Y, Male KB, Luong JHT (2004) Anal Chem 76:1083
28. Bard AJ, Faulkner LR (2001) Electrochemical methods fundamentals and applications. Wiley, New York
29. Nicholson RS, Shain I (1964) Anal Chem 36:706
30. Hu IF, Karweik DH, Kuwana T (1985) J Electroanal Chem 188:59
31. Zhang S, Wang N, Niu Y, Sun C (2005) Sens Actuat B 109:367
32. Lin WZ, Yi L, Ze Z (2003) Handbook of nanophase and nanostructured materials. Kluwer Academic/Plenum Publishers, New York
33. Zhang L, Jiang X, Wang E, Dong S (2005) Biosens Bioelectron 21:337
34. Farzinnejad N, Miran Beigi AA, Fotouhi L, Torkestani K, Ghadirian HA (2005) J Electroanal Chem 580:245
35. Schwarz WM, Shain I (1965) J Phys Chem 69:30
36. Rashwan F, Mohran H (1993) Bull Chem Soc Jpn 66:1871
37. Pospisil L, SoKolova R, Colombini MP, Giannarelli S, Fuoco R (2000) Microchem J 67:305